ACS APPLIED ENERGY MATERIALS

www.acsaem.org Article

Binder-Focused Approaches to Improve the Stability of Cathodes for CO_2 Electroreduction

Uzoma O. Nwabara, Anthony D. Hernandez, Danielle A. Henckel, Xinyi Chen, Emiliana R. Cofell, Michiel P. de-Heer, Sumit Verma, Andrew A. Gewirth, and Paul J. A. Kenis*

Cite This: *ACS Appl. Energy Mater.* 2021, 4, 5175–5186 Read Online

ACCESS | Metrics & More | Article Recommendations | Supporting Information

ABSTRACT: While the use of flow electrolyzers has enabled high selectivity (>80%) and activity (>200 mA cm^{-2}) in the reduction of CO_2 to value-added chemicals, the durability of these systems is still insufficient for feasibility at scale. A key component of flow electrolyzers, the gas diffusion electrode, must be hydrophobic and stable to maintain the triple phase boundary at the catalyst layer. The catalyst layer consists of an active catalyst and a binder to augment hydrophobicity and stability. Many CO_2 electrolysis systems utilize Nafion as the binder, yet, these cathodes are prone to carbonate formation and are often not stable beyond 20 h. Inspired by knowledge from other electrocatalysis applications, this paper explores alternatives to Nafion in the catalyst layer as well as different methods of catalyst layer preparation. Cathodes with a poly(tetrafluoroethylene) (PTFE) binder elude carbonate formation, although their performance still decreases over time. However, the addition of PTFE to Nafion (mixed binders) limited carbonate formation. Furthermore, we found that coating cathodes with a Sustainion ionomer over layer extends lifetimes, presumably by hindering carbonate formation. The characteristics of cathodes with these binders are further explored using surface-enhanced Raman spectroscopy to help explain their effect on the electroreduction of CO_2.

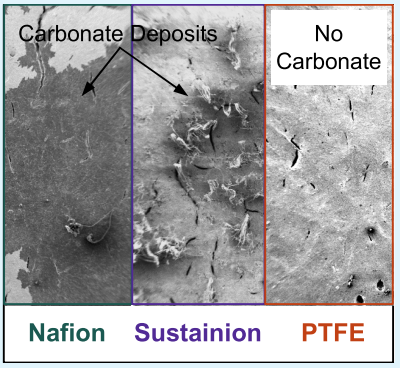

KEYWORDS: *CO_2 electroreduction, binders, stability, durability, degradation, gas diffusion electrodes*

1. INTRODUCTION

As the global population continues to increase, so does the demand for the natural resources that provide the energy, food, materials, *etc.* needed to support such populations.[1] The common, nonsustainable practices in place to meet such demands damage the earth's climate and delicate ecosystems. Many of these damages can be attributed to the increase in carbon emissions, such as atmospheric CO_2 levels, which is correlated with rising global temperatures. The concentration of CO_2 in the atmosphere has surpassed 410 ppm, and annual emissions have reached ~14.7 gigatons of CO_2 in excess of what nature can adsorb.[2] The majority of CO_2 emissions originate from industrial processes, operation of residential and commercial properties, electricity production, and transportation.[3] As a result, researchers have focused on developing technologies to curb emissions such as renewable energy production and electrification of transportation.

Researchers have turned their attention to curbing CO_2 emissions *via* the electrochemical reduction of CO_2 (ECO_2RR) to value-added chemicals and fuels like carbon monoxide (CO), methanol, formic acid, ethanol, methane, and ethylene.[4] Using renewable energy to drive ECO_2RR could create a carbon-neutral process. Moreover, ECO_2RR may offer an approach to store excess energy from intermittent renewable energies (wind, solar) in the form of liquid, high-energy-density chemicals. Seminal work by Hori *et al.* has shown that ECO_2RR product speciation is dependent on which electrocatalyst is used.[5] For example, Ag and Au will primarily produce CO, while Sn will produce formate.

To be considered for industrial integration, an ECO_2RR system must meet the following four benchmarks: (a) high current density or activity, (b) high faradaic efficiency (FE) or selectivity, (c) low overpotentials or high energetic efficiency, and (d) extensive durability/stability. All four benchmarks play an important role in determining the economic feasibility of an ECO_2RR process. Many researchers have succeeded in creating highly active and/or selective catalysts and systems for products such as CO (FE of >80%) and formate (>90%).[4,6] These products only require $2e^-$ (less electricity) and fewer reaction steps, in contrast with methane ($8e^-$), methanol ($6e^-$), ethylene ($12e^-$), and ethanol ($12e^-$). Systems or catalysts that selectively produce the latter, more energy-dense products at high activities are still required. Despite advances in product selectivity, durability is still a prominent issue in the ECO_2RR field. Without a long-lasting system, materials, in

Received: March 11, 2021
Accepted: April 20, 2021
Published: May 4, 2021

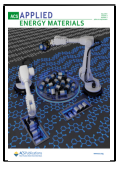

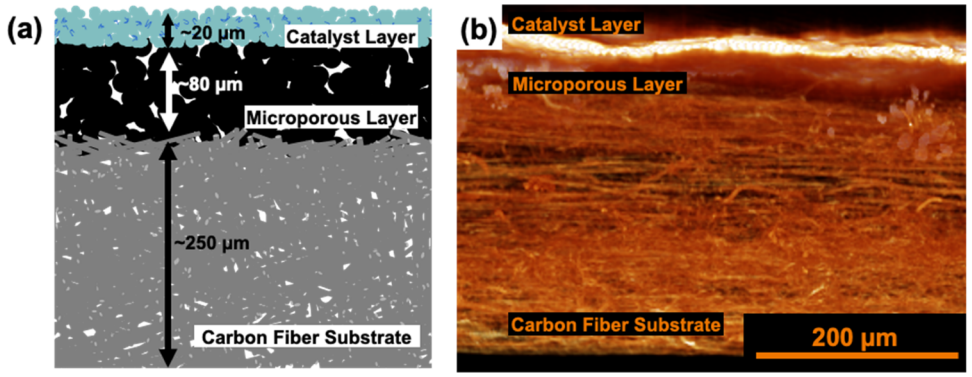

Figure 1. (a) Schematic detailing a standard gas diffusion electrode including the carbon fiber substrate, a microporous layer, and a catalyst layer and their approximate thicknesses.[27,28] The dark blue spots in the catalyst represent the distributed binder. (b) Corresponding micro-computed tomography (micro-CT) rendering of a gas diffusion electrode.

particular electrodes, would need to be replaced or undergo maintenance frequently, hampering the economics of the process.

ECO_2RR experiments are often conducted using a three-electrode cell setup. Yet, the solubility of CO_2 in aqueous solutions is poor (~35 mM at 20 °C),[7] leading to low mass transfer of CO_2 to the cathode which limits activity (<50 mA cm^{-2}). To address the issue of low solubility, research groups have developed membrane electrode assembly (MEA) and flow electrolyzers for ECO_2RR that utilize gas diffusion electrodes (GDEs) to eliminate the dependence on CO_2 solubility.[8−14] The use of GDEs is pivotal to the operation of such electrolyzers. As a result, the durability, and thus the economic feasibility, of ECO_2RR systems is dependent on the performance of GDEs.

A GDE typically consists of an electrocatalyst that has been deposited onto a gas diffusion layer (GDL, typically Teflon-treated carbon).[15,16] A schematic of the GDE is shown in Figure 1. CO_2 flows through the diffusion layer to the electrocatalyst where the reduction reaction occurs with the electrolyte at a triple phase boundary (TPB). The role of the GDL is to support the catalyst layer (CL) and to be hydrophobic enough to prevent the TPB from moving out of the CL (flooding). Flooding is one of the main failure mechanisms in a GDE-based flow electrolyzer because it impedes ECO_2RR activity and/or degrades system materials. Nevertheless, the CL also requires a degree of hydrophobicity to prevent flooding. The CL consists of the active catalyst, which can be hydrophilic and/or hydrophobic in nature, and a binder/ionomer, which holds the CL together and to the GDL. The binder promotes hydrophobicity and improves the durability of the GDE.

The CL is the first line of defense for flooding. If the binder degrades, then hydrophobicity is lost, causing flooding and degradation mechanisms such as leaching, where catalyst detaches and is lost to the liquid electrolyte.[6] A vast majority of researchers utilize Nafion (a perfluorosulfonic acid polymer) as a binder, but many ECO_2RR durability studies only show <100 h lifetimes, which fall shy of benchmarks (>1000 h) set by technoeconomic analyses.[6,17,18] From this, we realize that Nafion may not be the best binder and traditional CL deposition practices may not be sufficient for ECO_2RR when aiming for long lifetimes.

In this paper, we report a systematic investigation of how different binders used in the catalyst layers affect the durability of GDEs. We draw inspiration from the electrochemical field to identify, screen, and implement alternate catalyst layer binders in hopes of improving the performance and durability of the gas diffusion electrode. Many researchers have studied and incorporated polymers and binders into aspects of batteries, fuel cells, and solar cells to limit degradation and increase stability.[19−26] Since the CL is the thinnest layer (Figure 1), it requires proper tuning of properties such as wettability to maintain the TPB. Consequently, we explore strategies, including mixed binder cathodes and spin-coating ionomers onto the CL, as ways to augment stability. Incorporating *ex situ* and *in situ* characterization techniques provides us with information on the processes occurring on the cathode surface during electrolysis.

2. EXPERIMENTAL METHODS

2.1. Electrode Preparation. All electrodes were prepared using a previously described airbrushing setup starting with a Sigracet 35BC (Fuel Cell Store) GDL substrate.[29] At first, various binders were studied besides the catalysts by depositing the plain binders onto the GDL. Sustainion (Dioxide Materials, 5 wt %), Fumion (Fumatech, 3−8 wt %), and Nafion (Fuel Cell Earth, 5 wt %) were used as purchased. Poly(tetrafluoroethylene) (PTFE, Sigma-Aldrich, 60 wt % in water) and poly(vinylidene fluoride) (PVDF, Sigma-Aldrich, pellets) were first diluted to 5 wt % dispersions/solutions. Appropriate volumes of each binder solution were then measured and added to a vial with additional solvent (DI water for PTFE and Nafion, isopropanol for Nafion, ethanol for Sustainion, and dimethyl acetamide, DMAC, for Fumion and PVDF). The resulting mixture was then sonicated in a water bath for ~1 min before being airbrushed. The electrode was weighed before and after airbrushing to achieve a final loading of 1.0 ± 0.1 mg cm^{-2}. When PTFE is applied to the GDL alone, small particles are randomly dispersed on the surface rather than forming a film. Therefore, the PTFE GDL was heat-treated under flowing Ar gas at 250 °C for 2 h at a ramp rate of 2 °C min^{-1}.

Commercial Ag nanoparticles (NP) (Sigma-Aldrich, <100 nm, 99.5%) and IrO_2 NP (nonhydrate, Alfa Aesar) were airbrushed onto the substrate to create the cathode and anode, respectively. For the cathode, Ag powder, binder solution, and the corresponding solvents were added to a vial and then sonicated in a water bath for ~20 min. The resulting ink was then airbrushed onto the GDL. The volume of binder solution added was varied to give different binder weight percentages in the catalyst layer. Table S1 shows which solvents were used for each binder along with the weight percentages used in the catalyst layer. Since Ag is hydrophilic and some of the binders are highly hydrophobic (Fumion, PVDF), only a little water could be added to help disperse Ag. Too much water would cause the binder to crash out of solution. For the anode, IrO_2 powder, DI water, Nafion, and isopropanol were added to a vial and then sonicated in a water

https://doi.org/10.1021/acsaem.1c00715
ACS Appl. Energy Mater. 2021, 4, 5175−5186

bath for ∼20 min. The resulting ink was then airbrushed onto the GDL. The GDE was weighed before and after airbrushing to achieve a final loading of 1.0 ± 0.1 mg cm^{-2}. For any Ag electrodes with PTFE, the GDE was heat-treated under flowing Ar gas at 250 °C for 2 h at a ramp rate of 2 °C min^{-1}.

2.2. Spin-Coating. Cathode spin-coating was performed with a Headway Research, Inc PWM32 Microprocessor Sequence Controller. Prior to spin-coating, the cathode was weighed. The binder solution was then placed at the center of the spin coater and drop-cast on the surface of the cathode, ensuring that the entire surface was coated. The cathode was left to rest for a few seconds before spinning at a certain speed for 30 s to create an even thin layer. After spin-coating, the cathodes were left to air-dry in a fume hood for 24 h. The cathode was then weighed again to determine the mass of material deposited.

2.3. Characterization Methods. Micro-computed tomography (micro-CT) images were taken using the Xradia Bio Micro-CT. The images were taken at 40 kV and 8 W. The micro-CT was built from 721 images with an exposure time of 5 s. Scanning electron microscopy (SEM) images were taken using the JEOL 7000F. The acceleration voltage was 15.0 kV with a working distance of 10 mm. X-ray diffraction (XRD) patterns were obtained with a Bruker D8 Advance X-ray diffractometer. Electrochemical impedance spectroscopy (EIS) measurements were conducted with a Reference 600 Gamry potentiostat at 1.30 V vs Ag/AgCl with 14 points per decade scanned from 10 kHz to 1 Hz. The Nyquist plots were fitted to a "one circuit and solution resistance" model as an equivalent circuit using the Gamry Echem Analyst module. Figure S1 shows the equivalent circuit. The R_{cell} and R_{ct} values were obtained from the equivalent fit of the Nyquist plots.

2.4. Binder Screening.

(a) Hydrophobicity tests *via* contact angle measurements. The hydrophobicity of the as-prepared Ag cathodes with different (single) binders was measured *via* contact angle goniometer (Ramé-Hart model 250). Droplets (10 μL) of DI water, 1 M KOH (≥85%, Fischer Scientific), 1 M KCl (99%, Sigma-Aldrich), and 1 M $KHCO_3$ (99.7%, Sigma-Aldrich) were placed on several sections of the Ag cathodes to arrive at an average contact angle. Ag NP with 10 wt % Nafion and plain Ag NP with no binder were the controls. With PTFE, Sustainion, PVDF, and Fumion, the binder loading started at 5 wt % and was increased by 5% if one or more of the droplets were not stable.

(b) Stability tests *via* Raman spectroscopy: The stability of the different binders was determined by subjecting the binder GDLs to a high alkaline electrolyte and conducting Raman spectroscopy. Figure S2 shows a process diagram detailing the steps for this test. Once the binder layers were airbrushed onto the GDL, Raman spectra were recorded using a Nanophoton Raman 11 under a green laser (531.94 nm) to obtain the characteristic peaks of each binder. The binder GDL was then cut, placed in the flow cell, and exposed to flowing 1 M KOH for a total of 24 h. Throughout the experiment at 2, 8, 14, and 20 h, the exposure was paused, the electrode was removed, and Raman spectra were recorded to monitor any chemical and/or physical changes to the binder layer. Such changes would be marked by new peaks and augmentation or declines of existing characteristic peaks. After 24 h of exposure, a final Raman measurement was performed. Micro-CT images were collected before and after the exposure experiments to observe any changes in the binder layer distribution. This stability test was done twice for each binder to confirm any trend, using a newly airbrushed binder GDL each time.

2.5. CO_2 Electrolysis in an Alkaline Flow Cell. An alkaline electrochemical flow cell was utilized to test each GDE for the electrochemical reduction of CO_2 to CO.[9] The reactor is composed of a rectangular stainless steel cathode gas flow chamber and current collector, a rubber gasket, a polyether ether ketone (PEEK) electrolyte chamber, and a stainless steel anode current collector. All of the components are held together with a squeeze-action toggle plier clamp (McMaster Carr). The clamped cell is then hooked up to the potentiostat (Autolab PGSTAT-30) to run potentiostatic or galvanostatic experiments. Multimeters (Crenova, MS8233D) are then connected to the cell to measure cathode and anode potentials against an Ag/AgCl reference electrode (Basi, RE-5B). Gaseous CO_2 (Airgas) flows at 17 sccm through a flow controller (Smart-Trak 2, Sierra Instruments) to the gas chamber along the cathode where it diffuses through GDE to the CL. A pump pushes liquid electrolyte through the PEEK chamber. Where the CO_2 meets the liquid electrolyte is the TPB, ideally at the CL allowing CO_2 electroreduction to occur. Anions produced from the reaction then flow across the electrolyte to the anode, where oxygen evolution occurs. Gaseous products flow back through the GDE to an in-line gas chromatograph (GC, Thermo Finnigan Trace GC) furnished with a thermal conductivity detector. A pressure regulator (Cole Parmer, 00268TC) hooked up to a vacuum pump was set to 14.20 psig and placed downstream of GC to maintain a proper pressure balance in the flow cell and to continuously pull reduction products through the GC for injections. Products of the reduction were analyzed to determine the activity (partial current density) and the faradaic efficiency of the catalyst.

2.6. Electroanalysis Testing. The effectiveness of cathodes was first tested using a standard electrochemical CO_2 reduction experiment in the alkaline flow cell. The gas flow meter maintained the CO_2 flow while a syringe pump (Harvard Apparatus, PHD 2000) flowed 1 M KOH through the PEEK chamber at 0.5 mL min^{-1}. The potentiostat supplied a voltage (−1.75, −2.00, −2.25, −2.50, −2.75, −3.00, or −3.50 V) to the cell and recorded the current. The cell was left for 200 s to equilibrate and let the product stream cycle through the GC sample loop. At 200 s, the GC began taking injections every minute for a total of three to minimize error. Once the GC finished injections and analysis, the next potential was applied, and the process was repeated.

2.7. Durability Testing. After electroanalysis, the cathodes were subjected to a standard durability test in the alkaline flow cell.[6] The gas flow meter maintained the CO_2 flow, while a peristaltic pump (Cole Parmer, Masterflex L/S Digital Drive) flowed 2 M KOH through the PEEK chamber at 1.0 mL min^{-1}. The potentiostat supplied a constant current to the cell and recorded the corresponding cell potential. After leaving the cell for 200 s to equilibrate, the GC took three injections to mark t = 0. Injections were taken every 30 min, while the current continued to be applied to reach 6 h of testing. SEM images were taken before and after the durability test to observe any changes in the binder layer morphology. Whenever trends in faradaic efficiency and/or cell potential were not clear or there was a discrepancy in repeated experiments, additional data was collected to confirm results.

2.8. Surface-Enhanced Raman Spectroscopy (SERS). A custom spectroscopic Raman flow cell was used for *in situ* SERS measurements.[30] SERS measurements were performed as previously reported[31,32] with a 531.9 nm laser (B&W Tek) providing sample excitation at approximately 45° relative to an 85 mm f/1.2 collection lens (Canon). The scattered radiation was then focused using an f/3.3 lens to the 50 μm slit of a SpectraPro 2300i monochromator (Princeton Instruments) with grating of 1200 grooves mm^{-1}. The charge-coupled device (CCD) detector (Andor) was thermoelectrically cooled to −80 °C. The typical spectral resolution was estimated to be 6 cm^{-1}. Acquisition time was 1 s, and the total accumulation of scans was 120. CO_2 flow rates were maintained at 12 sccm with a mass flow controller (Smart-Trak 2, Sierra Instruments). The electrolyte flow was maintained at 0.5 mL min^{-1} with a syringe pump (Harvard Apparatus Pump 33). A Ag/AgCl reference (BASi, RE-5B) in the cell enabled direct measurement of the cathode potential.

3. RESULTS AND DISCUSSION

3.1. Evaluation of Binder with Respect to Wettability and Stability. Due to their use in fuel cell, battery, and

https://doi.org/10.1021/acsaem.1c00715
ACS Appl. Energy Mater. 2021, 4, 5175−5186

ECO_2RR research, we identified PTFE, PVDF, Fumion, and Sustainion as potential alternative binders to Nafion.[14,33−36] Binders require high hydrophobicity and stability to consider being used in a catalyst layer for ECO_2RR, and we evaluate these properties below.

3.1.1. Hydrophobicity Tests with Contact Angle Goniometer. For hydrophobicity testing, catalyst layers with binder weight percentages ranging from 5 and 15% were tested as needed for each binder (see Table S1). Figure 2 shows the contact angle results for the different electrodes along with Nafion and binder-less Ag controls obtained using different electrolytes. All electrodes exhibit contact angles >85° following exposure to DI water and $KHCO_3$ ($pH_{1\ M\ KHCO_3}$ = 8.56).[37] This >85° contact angle is associated with a hydrophobic interaction and suggests that all interfaces, including the binder-less Ag layer, are hydrophobic.[38] Electrodes exposed to H_2O and $KHCO_3$ were stable. However, following exposure to KOH, a more alkaline electrolyte ($pH_{1\ M\ KOH}$ = 13.54),[37] or KCl ($pH_{1\ M\ KCl}$ = 6.32),[37] several of the catalysts became discolored and the contact angle changed from nonzero values to approximately 0° (marked with an asterisk in Figure 2). Alternatively, the Sustainion and PTFE cathodes did not become discolored following KOH and KCl exposure and exhibited contact angles similar to those observed with H_2O or $KHCO_3$ exposure.

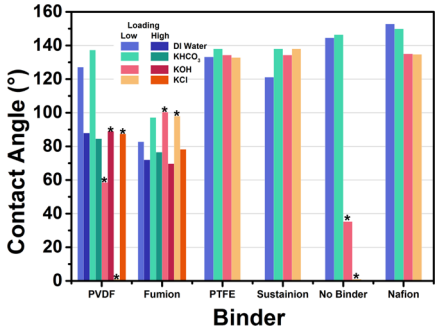

Figure 2. Contact angle measurements to characterize the hydrophobicity of various Ag NP GDEs with different electrolytes. The lighter and darker colors represent the lowest (5%) and highest (10 or 15%) binder weight percentages in the Ag catalyst layer, respectively. Data for a 10% Nafion Ag GDE and a binder-less Ag GDE are provided for comparison. Data labeled with * indicate electrodes on which the droplets eventually spread to 0° contact angle.

Previous studies have shown that, compared to neutral conditions, using alkaline electrolytes leads to higher activity for ECO_2RR.[37] A droplet spreading, rather than staying stationary, actually signifies an unstable, degrading electrode. In fact, studies have concluded that hydroxide ions can degrade PVDF membranes *via* dehydrofluorination.[39,40] We note that carbon−fluorine bonds are a common motif in binders/ionomers and membranes for ECO_2RR. The results above indicate that, in addition to providing hydrophobicity to ensure gas−liquid separation, binders can protect the catalyst from oxidation. Only PTFE and Sustainion displayed hydrophobicity comparable to the Nafion control (10 wt %) at lower weight percentages during KOH exposure.

3.1.2. Stability Tests with Raman Spectroscopy. Next, we used Raman spectroscopy to study the effect of flowing KOH on the different binders by evaluating the spectra over a 24 h exposure time (Figure S3). The characteristic peaks are identified in Table S2. Unexpectedly, none of the spectra show any major changes (such as carbon−carbon double-bond formation from dehydrofluorination) over the 24 h time course of the measurement, suggesting that all four binders are stable against the 1 M KOH electrolyte. This was confirmed when repeating the experiment with fresh binder-coated GDLs. Additionally, the micro-CT images (Figure S4) taken before and after 24 h of exposure reveal that the binder layers absent of incorporated Ag remain intact against flowing KOH and that no major changes occur in binder layer uniformity. We considered that small amounts of the binder may have come off the GDL and leached into the flowing KOH. Yet, no detectable traces of fluorine (PVDF, PTFE, Fumion) or chlorine (Sustainion) were found in the effluent KOH electrolyte using either inductively coupled plasma optical emission spectrometry (ICP-OES) or ^{19}F NMR.

3.2. Performance of Different Binders in CO_2 Electrolysis. *3.2.1. Electroanalysis.* The binder evaluation tests described above suggested that PTFE and Sustainion are promising catalyst layer binders due to their ability to maintain a hydrophobic surface in 1 M KOH. 5 wt % PTFE and 5 wt % Sustainion Ag GDEs along with 5 and 10 wt % Nafion Ag GDE controls were used to perform ECO_2RR in an alkaline flow electrolyzer. Figure 3a compares the current density from each electrode. As expected, PTFE exhibits the lowest current

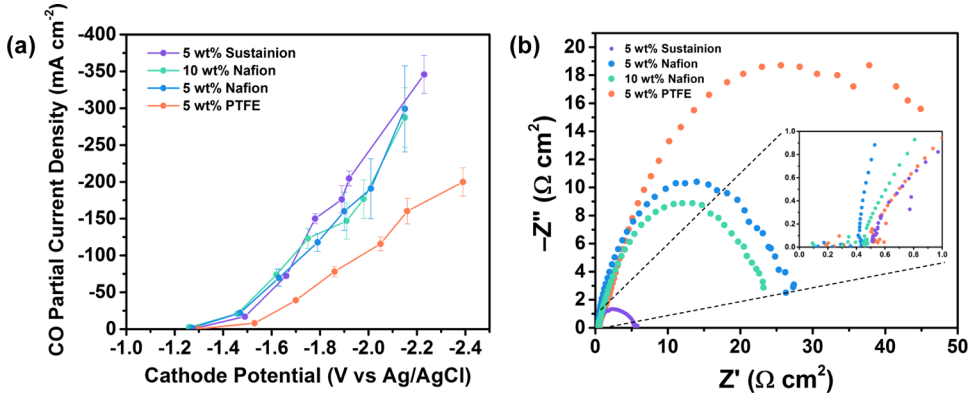

Figure 3. (a) Partial current density of CO from electrolysis experiments performed on Ag GDEs of various binders and binder loadings. (b) Electrochemical impedance spectroscopy data for the Ag electrodes with the different binders at −1.30 V vs Ag/AgCl; inset: expanded view of R_{cell} for each electrode near the origin. Anode: 1 mg cm^{-2} IrO_2; 1 M KOH@0.5 mL min^{-1}.

https://doi.org/10.1021/acsaem.1c00715
ACS Appl. Energy Mater. 2021, 4, 5175−5186

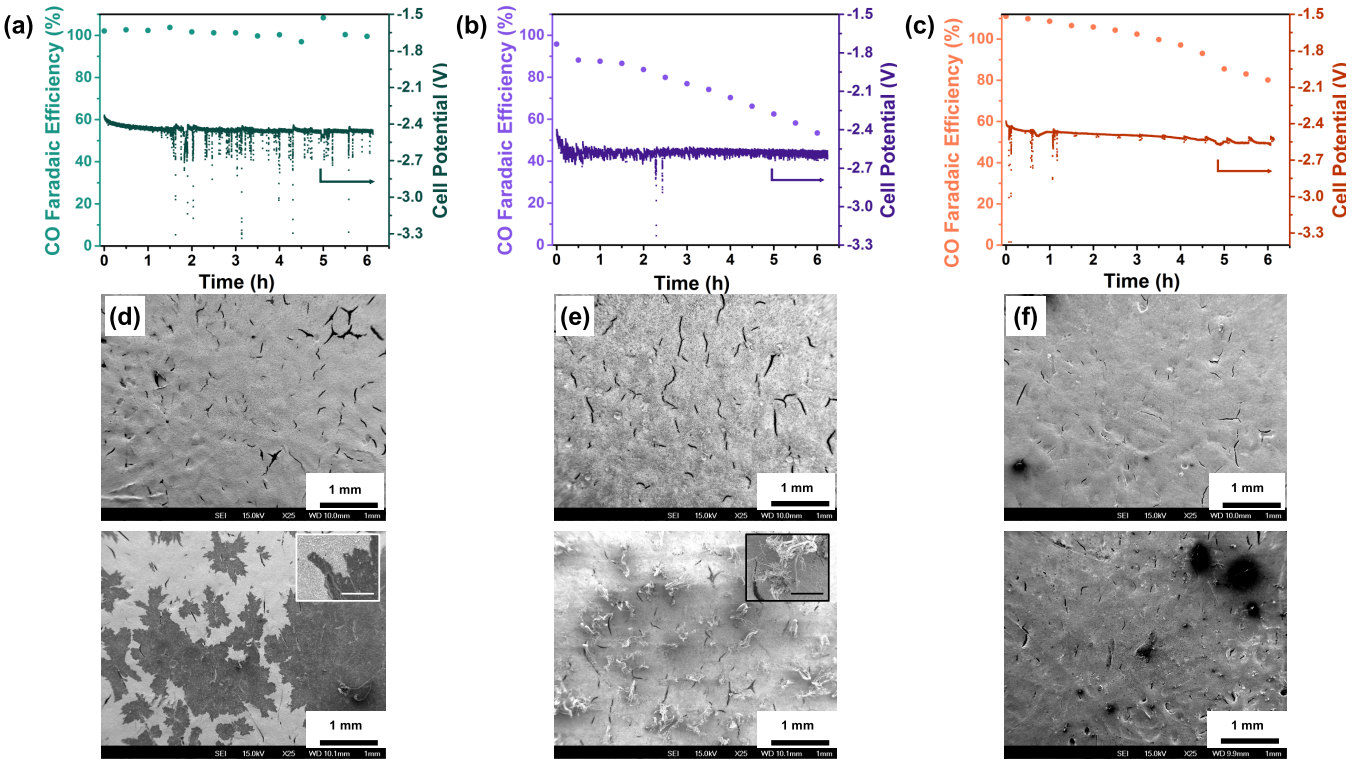

Figure 4. Plots of the CO faradaic efficiency and cell potential over 6 h durability tests for Ag GDEs with different binders: (a) 10% Nafion, (b) 5% Sustainion, and (c) 5% PTFE. The corresponding SEM images show the Ag surface before (top) and after (bottom) the durability tests for Ag GDEs with different binders: (d) 10% Nafion, (e) 5% Sustainion, and (f) 5% PTFE. The insets zoom in on the carbonate formations; the scale bars represent 50 μm. Anode: 1 mg cm^{-2} IrO_2; 2 M KOH@1 mL min^{-1}; −200 mA cm^{-2}.

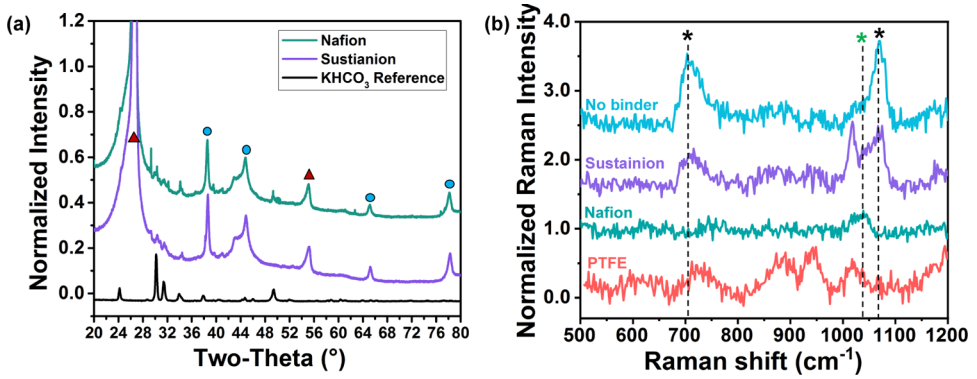

Figure 5. (a) Thin-film XRD pattern of used single-binder Ag GDEs with a $KHCO_3$ salt reference pattern. Red triangles: C; blue circles: Ag. (b) SERS spectra for fresh Ag GDEs with different single binders taken at open-circuit potential (OCP) in 1 M $KHCO_3$. The peaks at ∼700 and ∼1058 cm^{-1} indicated by the black * represent chemisorbed HCO_3^-, while the peak at ∼1020 cm^{-1} indicated by the green * represents HCO_3^- in solution.

density at all potentials compared to the other binders due to its lower conductivity.[41] The Sustainion electrode exhibited slightly better performance than the Nafion electrode at higher potentials (>−1.7 V vs Ag/AgCl).

To gain further insight, EIS was performed on each electrode during ECO_2RR and the resulting Nyquist plots are shown in Figure 3b. Fitting these Nyquist plots using a "one circuit and solution model" resulted in R_{ct} values of 4.83, 22.8, 25.9, and 67.3 Ω for the 5 wt % Sustainion, 10 wt % Nafion, 5 wt % Nafion, and 5 wt % PTFE cathodes, respectively. These values show substantial differences in R_{ct} between electrodes fabricated with the different binders. From the expanded view of the origin (inset in Figure 3b), we see that the R_{cell} values, which signify the internal resistance (contact and solution resistances) of the cell, for each electrode are relatively similar and do not differ as significantly as the R_{ct} values. Specifically, the R_{cell} values provided from Nyquist plot fittings were 0.45, 0.21, 0.22, and 0.31 Ω for the 5 wt % Sustainion, 10 wt % Nafion, 5 wt % Nafion, and 5 wt % PTFE cathodes, respectively. This result is expected since 1 M KOH was used for the characterization of each electrode, and slight variations in cell assembly and electrode preparation for each electrode due to human error and poor fitting may have contributed to these R_{cell} differences. Therefore, the EIS data suggest that Sustainion better facilitates ion transport at the electrode surface than Nafion and PTFE. Ion transport is key

https://doi.org/10.1021/acsaem.1c00715
ACS Appl. Energy Mater. 2021, 4, 5175−5186

in ECO_2RR, as OH^- generated at the cathode must be shuttled quickly to the anode to prevent a buildup, which would hinder kinetics.

3.2.2. Durability. Cathodes with Sustainion or PTFE binders were compared with a 10 wt % Nafion binder control in a standard durability test,[6] which was performed at a constant current of 200 mA cm^{-2} and 2 M KOH flowing at 1.0 mL min^{-1}. The durability performance for each cathode is shown in Figure 4a−c. The figure shows that the CO FE was maintained at ca. 100% for the Nafion control over the 6 h of testing. The high voltage transients seen after ca. 1.5 h are associated with nascent flooding of the electrode, which was confirmed visually. Both the Sustainion and PTFE cathodes exhibited ∼100% FE_{CO} at the start of the measurement, but the FE_{CO} declined by 20−50% at the 6 h mark, which was observed over multiple durability experiments.

To further understand the origin of degradation, we compared pre- and post-testing SEM images of the cathodes. Figure 4d shows that, prior to testing, the Nafion cathode exhibits an even catalyst layer albeit with the presence of small cracks associated with drying. Following ECO_2RR, SEM images reveal the presence of dark patches, associated previously with the presence of carbonate on the electrode. These carbonate deposits are known to lead to eventual electrode failure in flow and MEA-based electrolyzers alike.[6] SEM obtained from the Sustainion cathode (Figure 4e) also exhibited deposits but with a string-like morphology different from that observed from the Nafion cathode. XRD (Figure 5a) obtained from the Sustainion cathode exhibited peaks corresponding to $KHCO_3$ at ∼32, ∼34, and ∼50°. These peaks are also seen on the Nafion cathode, which exhibits clear evidence for $KHCO_3$ in the SEM. Lastly, SEM images from the PTFE cathode do not exhibit any evidence for a deposit on the surface or within the catalyst layer (at higher magnification). This observation suggests that PTFE withstands the formation of surface carbonates. The PTFE-bound CLs in H_2/air alkaline fuel cells also do not exhibit carbonate deposits.[42]

Looking at the performance of all cathodes, it is evident that the makeup of the catalyst layer greatly affects the degradation mechanism, which is carbonate formation in this case. In the water treatment field, added polymer-based inhibitors work to keep Ca^{2+} in the bulk solution and away from piping surfaces to avoid calcium carbonate deposition.[43,44] Hence, certain binders may possess properties that inhibit carbonate nucleation that naturally occurs on Ag during long-term electrolysis of CO_2. On the other hand, a binder may further promote the nucleation of carbonate. Specifically, a standard durability test completed for a Ag cathode without any binder exposes immediate performance loss. Figure S5 shows that the CO faradaic efficiency decreases throughout the entire 6 h, and the post-test SEM images reveal both catalyst leaching and carbonate formation. These results underscore the role of the binder to keep the catalyst together and bind it to the substrate along with discourage unwanted carbonate deposition.

3.2.3. Investigating Surface Species with Surface-Enhanced Raman Spectroscopy. Based on our results on the durability of Nafion, Sustainion, and PTFE Ag GDEs, we attempted to gain further insight on differences in degradation occurring on the respective electrodes. Surface-enhanced Raman spectroscopy (SERS) was performed on each Ag GDE along with a no-binder Ag GDE as a control. First, we wanted to understand the configuration of HCO_3^- on the surface of these electrodes using $KHCO_3$ electrolyte, since we identified this species comprising the deposits on the electrode surface seen in Figure 4d,e after durability testing. Initial measurements were taken at open-circuit potential (OCP), and then an additional experiment was completed under multiple applied potentials with flowing 1 M KOH. Figure 5b compares the OCP SERS data for the various GDEs with flowing $KHCO_3$ electrolyte. Peaks with black stars (∼700 and ∼1058 cm^{-1}) represent chemisorbed carbonate (HCO_3^-/CO_3^{2-} shared modes), while the peak with a green star (∼1025 cm^{-1}) represents HCO_3^- in solution.[45] The peaks at ∼700 and ∼1058 cm^{-1} could be due to either chemisorbed HCO_3^- or CO_3^{2-} as they share these modes, and we assume these peaks indicate HCO_3^- as this is the electrolyte composition. The chemisorbed HCO_3^- peak only appears when Sustainion or no binder is present in the catalyst layer when exposed to 1 M $KHCO_3$. This suggests that Ag characteristically adsorbs HCO_3^- and the presence of Sustainion does not affect this property of Ag. We expect Sustainion to permit the exchange of anions in solution as it is an anion exchange binder [and membrane], which makes it very attractive for MEA-based ECO_2RR cells. Nafion, however, appears to block the chemisorption of HCO_3^-, allowing it only to reside in the boundary layer and bulk solution; again, as a proton exchange binder, we expect this behavior from Nafion. Nafion maintains this property even under applied potentials (Figure S6). These data agree with the EIS data we collected: R_{ct} was lowest for Sustainion followed by Nafion suggesting good anion transport. Additionally, the blockage and free flow of anions exhibited by Nafion and Sustainion, respectively, may play a role in the local pH at the CL boundary layer, which would affect ECO_2RR product selectivity with catalysts that form multiple products (*i.e.*, Cu).

We now can contemplate the varying carbonate morphologies for each Ag GDE. When Nafion is present, HCO_3^- is limited to the boundary layer of the Ag GDE, which may explain why we observed carbonate settling atop the catalyst surface, possibly interacting with the Ag NPs to create planar coverage.[46] Nafion may shield the catalyst layer by hindering the flow of detrimental carbonate into the CL (and GDL), thus decelerating the clogging of pores and blockage of active sights. Considering the presence of $KHCO_3$ on both Nafion and Sustainion CLs, however, we understand that both HCO_3^- and K^+ must be present for carbonate to form on Ag NPs. Although Nafion prohibits anion flow, it allows for the free flow of cations (K^+) from the bulk electrolyte to the catalyst surface, thus providing a path for carbonate deposition. Again, water treatment research stresses keeping cations in bulk electrolyte when trying to avoid carbonate formation.[43] With Sustainion, the free exchange of HCO_3^- and lack of carbonate layers covering the Ag CL suggest that carbonate formation is occurring inside the GDE layers away from what can be observed with SEM, causing blocking of pores and active sites. The carbonate patches apparent when testing Ag without binder may be due to the poor hydrophobicity of the CL, which allows it to become fully wetted.

As shown in Figure 5b, conducting SERS on the PTFE Ag cathode at OCP under $KHCO_3$ revealed only solution HCO_3^- signals, similar to that observed for the Nafion Ag cathode. Note that SERS data were collected on unannealed PTFE Ag cathodes because the annealed cathode did not emit any Raman signal. Next, measurements were taken at OCP and then under multiple applied potentials with flowing 1 M KOH and 12 sccm CO_2. In general, we found that under alkaline

https://doi.org/10.1021/acsaem.1c00715
ACS Appl. Energy Mater. 2021, 4, 5175−5186

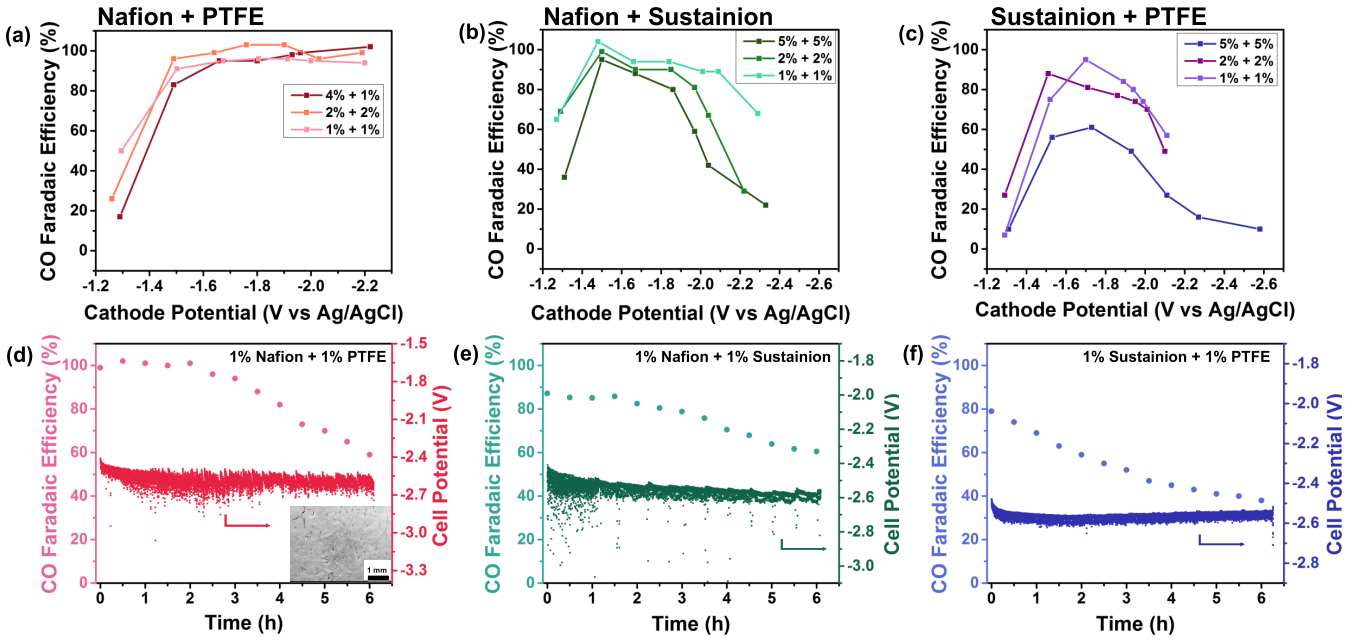

Figure 6. CO faradaic efficiency from CO_2 electrolysis experiments on Ag GDEs with mixed binders at different weight percentages in the catalyst layer: (a) Nafion + PTFE, (b) Nafion + Sustainion, and (c) Sustainion + PTFE. Anode: 1 mg cm^{-2} IrO_2; 1 M KOH@0.5 mL min^{-1}. Resulting CO FE (left axis) and cell potential (right axis) during a 6 h durability experiment for mixed binder Ag GDEs: (d) 1% Nafion + 1% PTFE, (e) 1% Nafion + 1% Sustainion, and (f) 1% Sustainion + 1% PTFE. Inset in (d): SEM image of the Ag surface after the durability test. No carbonate formation evident on top of the catalyst layer. Anode: 1 mg cm^{-2} IrO_2; 2 M KOH@1 mL min^{-1}; −200 mA cm^{-2}.

flowing conditions, the surface enhancement of the electrodes decreased, leading to a lack of enhancement seen most in the no-binder Ag GDE (Figure S6). When the Ag cathode with PTFE is exposed to 1 M KOH and 12 sccm CO_2, it exhibits chemisorbed HCO_3^-/CO_3^{2-} peaks along with the solution peak (Figure S6). These results do not fully explain the absence of carbonate on the PTFE cathode surface. Beckmann et al. stated that hydrophilic electrodes carbonize faster than hydrophobic electrodes.[47,48] PTFE is a polymer consisting of a carbon chain saturated with fluorine, resulting in a highly hydrophobic material.[49] Although it is sufficiently hydrophobic compared to the electrolyte (as confirmed by the contact angle measurements), Nafion contains sulfonate side chains that permit a certain degree of hydrophilicity important for proper electrode wetting.[33,50] Both Nafion and PTFE exhibited similar interactions with HCO_3^- and CO_3^{2-} from SERS, mainly showing solution-based peaks even at applied potentials. Therefore, the lack of carbonate formation on the cathode with PTFE may be attributed to the high hydrophobicity of PTFE along with its small amount of chemisorbed carbonates. In addition, the annealing step required for the PTFE cathodes may coat the Ag NPs in PTFE, thus shielding the Ag NP from carbonate deposits. Once coated, the poor electrical conductivity of PTFE may hinder the flow and concentration of HCO_3^- and K^+ near the Ag NPs, thus discouraging carbonate deposition and growth. This idea agrees with our EIS data (Figure 3b), which revealed a high charge transfer resistance for PTFE. In summary, the SERS data can help to explain the superior durability of electrodes with Nafion rather than Sustainion in the Ag CL and why carbonate morphologies appearing on the Ag surface are different for these binders.

3.3. CO_2 Electrolysis with Mixed Binder Cathodes. The aforementioned results and data characterize the nature and performance of all binders along with their benefits and setbacks. Nafion is stable, but prone to carbonate formation in the catalyst layer. Sustainion is an anion exchange ionomer, but brittle (cracks observed in micro-CT images, Figure S4) and unstable in performance as tested. Finally, PTFE is stable, flexible, and resists carbonate formation, but has very low conductivity. Looking closer, the benefits of some binders cancel out the setbacks of the others. Thus, we decided to investigate whether combining binders at different weight percentages would yield a better catalyst layer. Sustainion + PTFE (referred to as S + P) could offer a more conductive and flexible binder combination. Nafion + Sustainion (N + S) could reveal a synergetic effect between these two cation and anion exchange ionomers. Nafion + PTFE (N + P) could help prevent carbonate from covering the catalyst surface.

We initiated these experiments with the S + P and N + S cathodes using 5 wt % of each binder, first conducting electroanalysis to assure sufficient performance. We quickly found out that a too high weight percent of binder resulted in low porosity/permeability and too high of hydrophobicity. The CO faradaic efficiencies for these cathodes were much lower compared to our control Ag cathodes at all cell potentials. If the catalyst layer is too hydrophobic, then the necessary supply of electrolyte cannot reach catalyst NPs to provide H_2O needed for CO_2 reduction. If the catalyst layer has low porosity, then any gaseous CO created cannot diffuse back through the GDL and be analyzed at the GC; instead, it escapes into the flowing electrolyte. To rectify this issue, the weight percent of each binder was continuously decreased, causing the FE_{CO} to increase with each new cathode. Figure 6a–c shows the electroanalysis results for each combination of N + P, N + S, and S + P cathodes. The 1% combinations exhibited the best results for the N + S and S + P cathodes even though the FEs were not above 90% for most of the applied potentials. Therefore, we performed standard durability tests on these 1% combination cathodes; the current was held at 200 mA cm^{-2} for the N + P and N + S cathodes and at

https://doi.org/10.1021/acsaem.1c00715
ACS Appl. Energy Mater. 2021, 4, 5175−5186

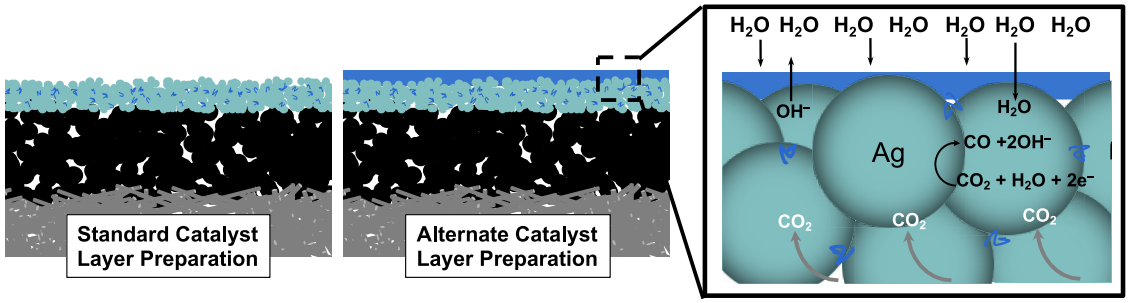

Figure 7. Visual explanation of the alternate catalyst layer design and preparation for our GDE. Our standard preparation involves coating the GDL with a catalyst with a binder incorporated into the ink. Our proposed design involves first preparing the standard GDE and then coating it with a layer of anion exchange binder (Sustainion) of ∼1 μm (see the Supporting Information for thickness calculation) to protect the active catalyst from degradation. Zooming in, we see a limit to the amount of water allowed to Ag active sites to create CO from CO_2.

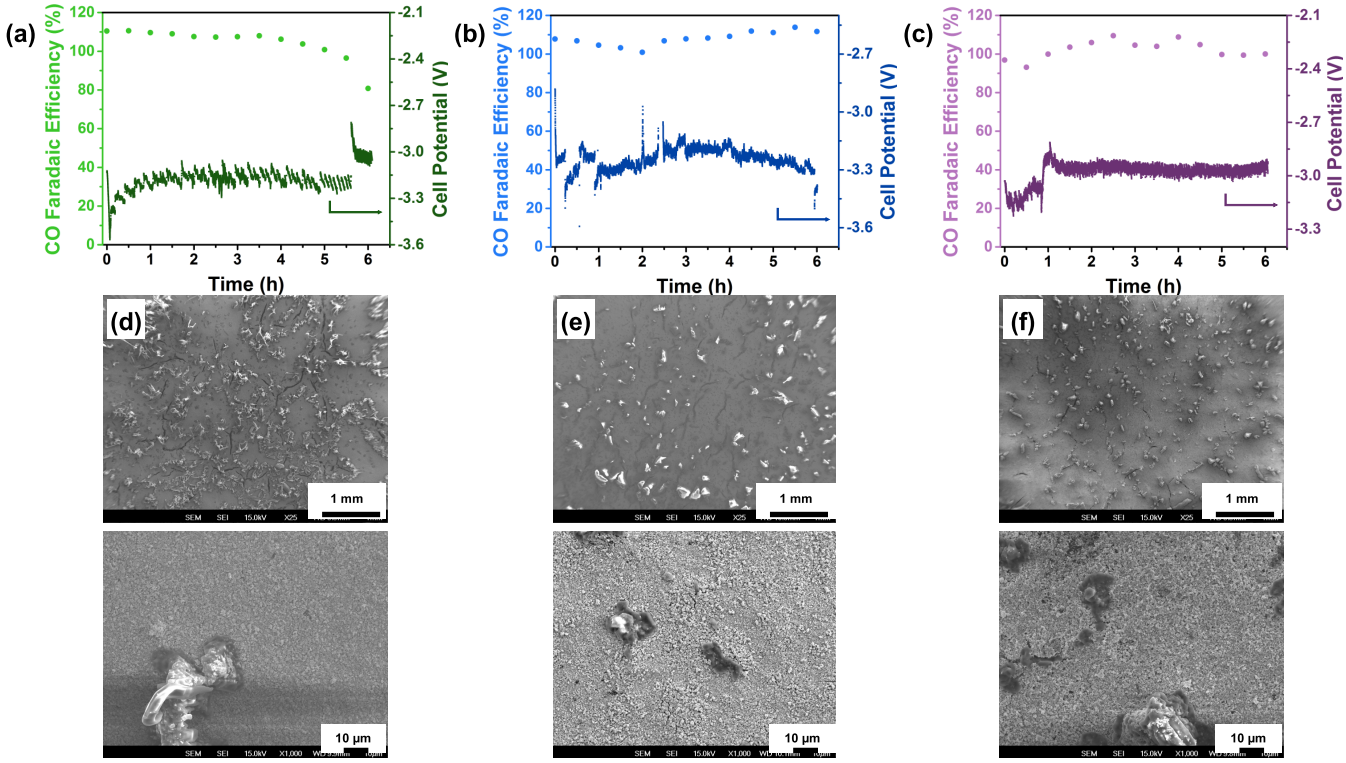

Figure 8. Testing with a larger inlet flow cell. Plots of the CO faradaic efficiency and cell potential over time as a result of the 6 h durability tests on Ag GDEs with various weight percentages of Nafion in the catalyst layer and then Sustainion spin-coated on top: (a) no binder, (b) 1% Nafion, and (c) 10% Nafion. SEM images show the CL after the durability testing: (d) no binder, (e) 1% Nafion, and (f) 10% Nafion. Anode: 1 mg cm^{-2} IrO_2; 2 M KOH@1 mL min^{-1}; −200 mA cm^{-2}; Sustainion: 100 μL, 500 rpm.

150 mA cm^{-2} for the S + P cathode to ensure >90% FE_{CO}. As shown in Figure 6d–f, the CO faradaic efficiency decreases over the 6 h testing period for all three cathodes. Once mixed and at such a low weight percent, the performance of the Nafion cathode seems to no longer retain its durability. Surprisingly, adding Sustainion seems to negatively impact both Nafion and PTFE, both of which exhibited better durability than Sustainion when tested alone.

The N + P Ag cathodes, tested last, showed surprisingly different results. With knowledge from the performance of the N + S and S + P cathodes, we started with a 1 wt % combination for the N + P. The electroanalysis data depicted in Figure 6a revealed higher FE_{CO} at all applied cell potentials than the other binder mixtures indicating no obvious hydrophobicity or porosity issues. The 6 h durability study with the 1 wt % N + P cathode illustrated in Figure 6d revealed that the FE_{CO} remained stable for ∼2 h before it unfortunately declined for the remainder of the test. The other N + P combination cathodes were also durability tested but did not exhibit enhanced durability (Figure S5). Using SEM, however, we were able to view any variations of the catalyst surface. Like we observed with the 5 wt % PTFE Ag cathode, carbonate did not precipitate on the surface of the N + P cathode (inset in Figure 6d).

Mixing and/or annealing binders may cause changes in their properties. For example, Nafion membranes utilized for fuel cells tend to melt and recrystallize under various annealing temperatures from 120 to 270 °C.[51−53] One study showed that water uptake was directly proportional to the treatment temperature of the Nafion membrane.[52] This phenomenon may have occurred with the Nafion in the N + P cathode, which was heated to disperse the PTFE, thus causing Nafion to

https://doi.org/10.1021/acsaem.1c00715
ACS Appl. Energy Mater. 2021, 4, 5175−5186

change its properties and leading to a loss in ECO_2RR durability. Just mixing the binders when preparing the catalyst ink for airbrushing may also impact each binder's properties. Ultimately, trying to compensate for the flaws of each binder by mixing them may not be the most sufficient way, but it does provide insight on important properties that need to be considered when designing new materials.

3.4. Sustainion-Coated Cathodes. *3.4.1. Justification for Coated Cathode Design.* When considering the lifetimes exhibited by the ECO_2RR cathodes studied, carbonate formation and electrolyte flooding are usually the only degradation mechanisms we observe. A strategy that would protect the catalyst surface against these two degradation mechanisms is expected to improve electrochemical durability. The augmented durability would reveal and enable the study of other degradation mechanisms presently obscured by carbonate formation and flooding. Carbonate is so prone to forming on the Ag cathodes mainly because of the abundance of OH^- ions supplied by the KOH electrolyte (eq 1) and the ECO_2RR.[54−56] Alternatively, using $KHCO_3$ as an electrolyte may limit carbonate formation but decreases energy efficiency and FE_{CO}.[37,57] When using $KHCO_3$ or K_2CO_3 as the electrolyte, the FE_{CO} decreased over the 6 h durability testing and carbonate still formed on the cathode surfaces.[58] Again, flooding occurs when the electrode is not sufficiently hydrophobic to maintain the triple phase boundary at the catalyst layer. Taking this into account, effectively controlling the amount of aqueous electrolyte (and therefore abundant OH^-) that reaches the catalyst layer would hopefully curb carbonate formation and flooding.

$$CO_2(aq) + OH^- \rightleftharpoons HCO_3^-(aq); \quad K = 4 \times 10^7 \qquad (1)$$

The orthodox catalyst layer preparation involves uniformly incorporating the binder into the CL itself. An alternative approach would be to apply a thin layer (*i.e.*, 0.7−2.0 μm) of binder directly on top of the traditional CL (Figure 7). Researchers in both the fuel cell and ECO_2RR fields have coated carbon supports and catalysts with ionomers to increase stability.[25,26,59,60] No binder is perfectly hydrophobic, meaning the binder layer would allow some electrolyte (OH^- and water) to reach the catalyst layer for ECO_2RR. ECO_2RR makes OH^-, which needs to be shuttled to the anode and oxidized to complete to full reaction. Therefore, the binder layer must be anion exchanging, ruling out Nafion and PTFE. Any water that does reach the catalyst layer would ideally react to form CO before causing flooding. The Raman spectra from the stability screening test (see above) revealed that all binders in plain layers were able to withstand prolonged exposure to KOH. Therefore, out of the remaining options, Fumion, PVDF, and Sustainion, we chose Sustainion as a coating binder layer.

3.4.2. Performance of Sustainion-Coated Cathodes. The main variables we considered for this alternative catalyst layer design were binder loading in the CL and the binder layer thickness. Precise tuning is important to avoid the GDE becoming too hydrophobic. We tested the Sustainion-coated approach for four different cathodes: 1% Nafion, 10% Nafion, 5% PTFE, and no binder. The Sustainion coatings were applied *via* spin-coating. Solution volumes and spinning speeds were varied to alter the layer thickness. Figure 8a−c shows the performance of a few combinations from durability testing. Note that these tests were conducted with a larger inlet flow cell (Figure S8) to avoid the clogging at the CO_2 inlet observed in our standard flow cell (Figure S9b). Coating the CL with Sustainion preserved the stable electrochemical performance originally observed for the Nafion Ag GDE (Figure 4a). Moreover, it improved the performance of the original Ag GDE without binder (Figure S9a). More importantly, through SEM (Figure 8d−f), we observed a lower carbonate coverage of the CLs of these GDEs, also verified by XRD (Figure S10), suggesting that the spin-coated Sustainion layer aided in hampering carbonate formation. Impeding this degradation mechanism led to an improvement in the stability of the cathodes.

Additionally, we attempted to optimize the design of this alternative CL design. The data in Figure 8 are from Ag cathodes spin-coated with 100 μL of Sustainion at 500 rpm, which resulted in a Sustainion layer thickness of ∼1.0 μm (see calculation in the Supporting Information). By varying the process parameters, we also obtained GDEs with thicker Sustainion coatings, but these did not perform well in electrochemical durability testing. The thicker layers were too hydrophobic, which disallowed proper wetting of the catalyst layer. Once again, we obtained low FE_{CO} similar to when we tested the mixed binder GDEs with high binder loading. The durability test results from the spin-coated cathode with 5% PTFE are given in Figure S9c. Even though the CO faradaic efficiency still decreases over time, the presence of the Sustainion coating compelled the 5% PTFE cathode to degrade at a slower rate, a similar effect observed with the spin-coated no-binder cathode (Figure 8a). Yet, again the 5% PTFE cathode did not exhibit visible carbonate formation on the electrode surface (Figure S9d), revealing a promising path for catalyst layer design for improved stability.

4. CONCLUSIONS

In this work, we aimed to identify optimal binders for catalyst layers in GDEs used for the electroreduction of CO_2 to value-added chemicals and fuels. First, we studied and evaluated potential replacements for the state-of-the-art binder, Nafion, using hydrophobicity (contact angle) and stability (Raman spectroscopy) tests. Binders with sufficient hydrophobicity and stability were then incorporated into Ag catalyst layers to create GDEs for electroanalysis and standard durability tests. The behaviors of these binders in GDEs for ECO_2RR were also evaluated using EIS and SERS. Finally, we designed more stable GDEs using combinations of binders in the catalyst layers or coating deposited catalyst layers with Sustainion.

Sustainion and PTFE were stable under flowing KOH as their characteristic Raman peaks did not change over 24 h of testing. Their hydrophobicity was comparable to that of Nafion for all tested electrolyte droplets, thus revealing their ability to control the triple phase boundary at the CL. Although Nafion Ag GDEs proved to be the most durable binder throughout the durability testing in terms of CO faradaic efficiency, SEM images indicated that the cathode degraded *via* carbonate formation, verified by XRD. Sustainion Ag GDEs were the least durable of the binder-incorporated electrodes and also exhibited carbonate formation on the CL surface. CLs with a PTFE binder were found to elude carbonate formation, although their ECO_2RR performance decreased over time. Cathodes with Sustainion, an anion exchange binder, showed the least charge transfer resistance when characterized using EIS. This trait was further explained by SERS, which indicated that Sustainion allowed for the free flow of carbonate ions (chemisorbed HCO_3^-/CO_3^{2-} peaks) through the CL. SERS with Nafion and PTFE Ag GDEs, however, blocked the

https://doi.org/10.1021/acsaem.1c00715
ACS Appl. Energy Mater. 2021, 4, 5175−5186

absorption of carbonate (showing solution HCO_3^- peaks), thus offering insight on the varying degrees of carbonate formation for each tested cathode. The use of combinations of binders in the CLs did not improve durability, but adding PTFE to Nafion in the CL eliminated carbonate formation typical of cathodes with just Nafion. By coating Ag GDEs with a Sustainion overlayer, we can enhance cathode stability while maintaining its performance; these Sustainion-coated cathodes hindered carbonate formation.

The ultimate goal of this work is to gain insight necessary for designing more stable GDEs to augment ECO_2RR lifetimes. These studies were conducted for a flow electrolyzer, but we hypothesize that the results and conclusions drawn would apply to MEA-based ECO_2RR cells as well. Further improvements in performance can be achieved by identifying, evaluating, and incorporating new binders in the CL to hopefully improve cathode durability and stability. Moreover, different binders may also affect local pH at Cu catalyst layers and thus product selectivity.[55] In addition, spin-coating other anion exchange binders such as Fumion or PVDF over the GDE instead of Sustainion may hinder or even prevent failure mechanisms and thus improve durability. With better designed CLs, GDEs can be pushed toward longer lifetimes, therefore moving ECO_2RR in the direction of economic feasibility.

■ ASSOCIATED CONTENT

Supporting Information

The Supporting Information is available free of charge at https://pubs.acs.org/doi/10.1021/acsaem.1c00715.

> Binder weight percentages and appropriate solvent and solvent ratios for airbrushing; equivalent circuit for EIS fitting; flow diagram for Raman stability experiment; Raman spectra of binders throughout KOH exposure and identification of characteristic peaks; micro-CT images before and after KOH exposure; durability test plots and SEM images for cathode without binder; SERS spectra of cathodes with different binders under applied potential and flowing CO_2; durability tests plots for mixed N + P binder cathodes; comparison of standard flow electrolyzer to large inlet flow electrolyzer; durability test plots and SEM images for spin-coated cathodes; and XRD patterns of spin-coated cathodes post durability testing (PDF)

■ AUTHOR INFORMATION

Corresponding Author

Paul J. A. Kenis − *Chemical and Biomolecular Engineering, University of Illinois at Urbana−Champaign, Urbana, Illinois 61801, United States;* orcid.org/0000-0001-7348-0381; Email: Kenis kenis@illinois.edu

Authors

Uzoma O. Nwabara − *Chemical and Biomolecular Engineering, University of Illinois at Urbana−Champaign, Urbana, Illinois 61801, United States*

Anthony D. Hernandez − *Chemical and Biomolecular Engineering, University of Illinois at Urbana−Champaign, Urbana, Illinois 61801, United States*

Danielle A. Henckel − *Chemical and Biomolecular Engineering, University of Illinois at Urbana−Champaign, Urbana, Illinois 61801, United States; Chemistry, University of Illinois at Urbana−Champaign, Urbana, Illinois 61801, United States*

Xinyi Chen − *Chemistry, University of Illinois at Urbana−Champaign, Urbana, Illinois 61801, United States;* orcid.org/0000-0002-6990-5233

Emiliana R. Cofell − *Chemical and Biomolecular Engineering, University of Illinois at Urbana−Champaign, Urbana, Illinois 61801, United States; Material Science and Engineering, University of Illinois at Urbana−Champaign, Urbana, Illinois 61801, United States*

Michiel P. de-Heer − *Shell Global Solutions International B.V., 1031 HW Amsterdam, The Netherlands*

Sumit Verma − *Shell International Exploration and Production Inc., Houston, Texas 77082, United States;* orcid.org/0000-0001-8365-180X

Andrew A. Gewirth − *Chemistry, University of Illinois at Urbana−Champaign, Urbana, Illinois 61801, United States;* orcid.org/0000-0003-4400-9907

Complete contact information is available at: https://pubs.acs.org/10.1021/acsaem.1c00715

Notes

The authors declare no competing financial interest.

■ ACKNOWLEDGMENTS

The authors gratefully acknowledge Shell's New Energies Research and Technology (NERT) Dense Energy Carriers program for providing funding for this work. They also acknowledge the International Institute of Carbon Neutral Energy Research (WPI-I2CNER) sponsored by the Japanese Ministry for Education, Culture, Sports, Science and Technology; the SURGE Fellowship; the 3M Corporate Fellowship; and the Dupont Science and Engineering Fellowship for the funding of UON. The authors also acknowledge the user facilities at the Materials Research Laboratory and the Beckman Institute at the University of Illinois. Finally, they acknowledge the Hong Yang group at the University of Illinois for use of their lab equipment, Jimmy Jang for performing the spin-coating, and Saket Bhargava for helping to analyze some data.

■ REFERENCES

(1) United States Energy Information Administration. International Energy Outlook, 2018. https://www.eia.gov/outlooks/ieo/.

(2) Intergovernmental Panel on Climate Change. *Synthesis Report Summary for Policymakers*; IPCC 2014. https://www.ipcc.ch/pdf/assessment-report/ar5/syr/AR5_SYR_FINAL_SPM.pdf.

(3) United States Environmental Protection Agency. *Source of Greenhouse Gases*; U.S. EPA, 2016.

(4) Jhong, H.-R.; Ma, S. C.; Kenis, P. J. A. Electrochemical conversion of CO_2 to useful chemicals: current status, remaining challenges, and future opportunities. *Curr. Opin. Chem. Eng.* **2013**, *2*, 191−199.

(5) Hori, Y. Electrochemical CO_2 Reduction on Metal Electrodes. In *Modern Aspects of Electrochemistry*; Vayenas, C. G. et al., Eds.; Springer: New York, NY, 2008; Vol. *42*, pp 89−189.

(6) Nwabara, U. O.; Cofell, E. R.; Kenis, P. J. A.; Verma, S.; Negro, E. Durable Cathodes and Electrolyzers for the Efficient Aqueous Electrochemical Reduction of CO_2. *ChemSusChem* **2020**, *13*, 855−875.

(7) Haynes, W. M., Eds. *CRC Handbook of Chemistry and Physics*, 91st ed.; Taylor & Francis Group, 2010; p 2800.

(8) Dodds, W. S.; Stutzman, L. F.; Sollami, B. J. Carbon Dioxide Solubility in Water. *Ind. Eng. Chem. Data Ser.* **1956**, *1*, 92.

(9) Ma, S.; Sadakiyo, M.; Luo, R.; Heima, M.; Yamauchi, M.; Kenis, P. J. A. One-step electrosynthesis of ethylene and ethanol from CO2 in an alkaline electrolyzer. *J. Power Sources* **2016**, *301*, 219−228.
(10) Luc, W.; Rosen, J.; Jiao, F. An Ir-based anode for a practical CO2 electrolyzer. *Catal. Today* **2017**, *288*, 79−84.
(11) Haas, T.; Krause, R.; Weber, R.; Demler, M.; Schmid, G. Technical photosynthesis involving CO2 electrolysis and fermentation. *Nat. Catal.* **2018**, *1*, 32−39.
(12) Dinh, C. T.; Burdyny, T.; Kibria, M. G.; Seifitokaldani, A.; Gabardo, C. M.; de Arquer, F. P. G.; Kiani, A.; Edwards, J. P.; De Luna, P.; Bushuyev, O. S.; Zou, C. Q.; Quintero-Bermudez, R.; Pang, Y. J.; Sinton, D.; Sargent, E. H. CO_2 electroreduction to ethylene via hydroxide-mediated copper catalysis at an abrupt interface. *Science* **2018**, *360*, 783−787.
(13) Yang, H. Z.; Kaczur, J. J.; Sajjad, S. D.; Masel, R. I. Electrochemical conversion of CO2 to formic acid utilizing Sustainion (TM) membranes. *J. CO_2 Util.* **2017**, *20*, 208−217.
(14) Kutz, R. B.; Chen, Q. M.; Yang, H. Z.; Sajjad, S. D.; Liu, Z. C.; Masel, I. R. Sustainion Imidazolium-Functionalized Polymers for Carbon Dioxide Electrolysis. *Energy Technol.* **2017**, *5*, 929−936.
(15) Kim, B.; Hillman, F.; Ariyoshi, M.; Fujikawa, S.; Kenis, P. J. A. Effects of composition of the micro porous layer and the substrate on performance in the electrochemical reduction of CO2 to CO. *J. Power Sources* **2016**, *312*, 192−198.
(16) Verma, S.; Nwabara, U. O.; Kenis, P. J. A. Carbon-Based Electrodes and Catalysts for the Electroreduction of Carbon Dioxide (CO2) to Value-Added Chemicals. *Nanostruct. Sci. Technol.* **2019**, 219−251.
(17) Verma, S.; Kim, B.; Jhong, H.; Ma, S. C.; Kenis, P. J. A. A Gross-Margin Model for Defining Technoeconomic Benchmarks in the Electroreduction of CO2. *ChemSusChem* **2016**, *9*, 1972−1979.
(18) Jouny, M.; Luc, W.; Jiao, F. General Techno-Economic Analysis of CO2 Electrolysis Systems. *Ind. Eng. Chem. Res.* **2018**, *57*, 2165−2177.
(19) Wang, R.-Y.; Kang, H.; Park, M. J. High-Capacity, Sustainable Lithium−Sulfur Batteries Based on Multifunctional Polymer Binders. *ACS Appl. Energy Mater.* **2021**, *4*, 2696−2706.
(20) Ha, T. A.; Li, H.; Wang, X.; O'Dell, L. A.; Forsyth, M.; Pozo-Gonzalo, C.; Howlett, P. C. Functional Binders Based on Polymeric Ionic Liquids for Sodium Oxygen Batteries Using Ionic Liquid Electrolytes. *ACS Appl. Energy Mater.* **2021**, *4*, 434−444.
(21) Lim, W.-G.; Oh, S.; Jeong, J.; Jang, W.; Shim, K. I.; Kim, S.; Han, J. W.; Im, S. G.; Lee, J. Ultrathin and Bifunctional Polymer-Nanolayer-Embedded Separator to Simultaneously Alleviate Li Dendrite Growth and Polysulfide Crossover in Li−S Batteries. *ACS Appl. Energy Mater.* **2021**, *4*, 611−622.
(22) Zhang, J.; Zhong, Y.; Wang, S.; Han, D.; Xiao, M.; Sun, L.; Meng, Y. Artificial Single-Ion Conducting Polymer Solid Electrolyte Interphase Layer toward Highly Stable Lithium Anode. *ACS Appl. Energy Mater.* **2021**, *4*, 862−869.
(23) Bella, F.; Verna, A.; Gerbaldi, C. Patterning dye-sensitized solar cell photoanodes through a polymeric approach: A perspective. *Mater. Sci. Semicond. Process.* **2018**, *73*, 92−98.
(24) Fagiolari, L.; Bonomo, M.; Cognetti, A.; Meligrana, G.; Gerbaldi, C.; Barolo, C.; Bella, F. Photoanodes for Aqueous Solar Cells: Exploring Additives and Formulations Starting from a Commercial TiO2 Paste. *ChemSusChem* **2020**, *13*, 6562−6573.
(25) Scibioh, M. A.; Oh, I.-H.; Lim, T.-H.; Hong, S.-A.; Ha, H. Y. Investigation of various ionomer-coated carbon supports for direct methanol fuel cell applications. *Appl. Catal., B* **2008**, *77*, 373−385.
(26) Breitwieser, M.; Bayer, T.; Büchler, A.; Zengerle, R.; Lyth, S. M.; Thiele, S. A fully spray-coated fuel cell membrane electrode assembly using Aquivion ionomer with a graphene oxide/cerium oxide interlayer. *J. Power Sources* **2017**, *351*, 145−150.
(27) Cofell, E. R.; Nwabara, U. O.; Bhargava, S. S.; Henckel, D. E.; Kenis, P. J. A. Investigation of Electrolyte-Dependent Carbonate Formation on Gas Diffusion Electrodes for CO_2 Electrolysis. *ACS Appl. Mater. Interfaces* **2021**, *13*, 15132−15142.
(28) Sigracet GDL 34 & 35 Series Gas Diffusion Layer. https://www.fuelcellstore.com/spec-sheets/SGL-GDL_34-35.pdf.
(29) Jhong, H.-R.; Brushett, F. R.; Kenis, P. J. A. The Effects of Catalyst Layer Deposition Methodology on Electrode Performance. *Adv. Energy Mater.* **2013**, *3*, 589−599.
(30) Chen, X.; Henckel, D. A.; Nwabara, U. O.; Li, Y.; Frenkel, A. I.; Fister, T. T.; Kenis, P. J. A.; Gewirth, A. A. Controlling Speciation during CO2 Reduction on Cu-Alloy Electrodes. *ACS Catal.* **2020**, *10*, 672−682.
(31) Rooney, R. T.; Schmitt, K. G.; von Horsten, H. F.; Schmidt, R.; Gewirth, A. A. Raman and QCM Studies of PPG and PEG Adsorption on Cu Electrode Surfaces. *J. Electrochem. Soc.* **2018**, *165*, D687−D695.
(32) Rooney, R. T.; Jha, H.; Rohde, D.; Schmidt, R.; Gewirth, A. A. Suppression of Copper Electrodeposition by PEG in Methanesulfonic Acid Electrolytes. *J. Electrochem. Soc.* **2019**, *166*, D551−D558.
(33) Naughton, M. S.; Gu, G. H.; Moradia, A. A.; Kenis, P. J. A. Tailoring electrode hydrophobicity to improve anode performance in alkaline media. *J. Power Sources* **2013**, *242*, 581−588.
(34) Danner, T.; Eswara, S.; Schulz, V. P.; Latz, A. Characterization of gas diffusion electrodes for metal-air batteries. *J. Power Sources* **2016**, *324*, 646−656.
(35) Papp, J. K.; Forster, J. D.; Burke, C. M.; Kim, H. W.; Luntz, A. C.; Shelby, R. M.; Urban, J. J.; McCloskey, B. D. Poly(vinylidene fluoride) (PVDF) Binder Degradation in Li-O2 Batteries: A Consideration for the Characterization of Lithium Superoxide. *J. Phys. Chem. Lett.* **2017**, *8*, 1169−1174.
(36) Jhong, H.-R.; Brushett, F. R.; Yin, L. L.; Stevenson, D. M.; Kenis, P. J. A. Combining Structural and Electrochemical Analysis of Electrodes Using Micro-Computed Tomography and a Microfluidic Fuel Cell. *J. Electrochem. Soc.* **2012**, *159*, B292−B298.
(37) Verma, S.; Lu, X.; Ma, S. C.; Masel, R. I.; Kenis, P. J. A. The effect of electrolyte composition on the electroreduction of CO_2 to CO on Ag based gas diffusion electrodes. *Phys. Chem. Chem. Phys.* **2016**, *18*, 7075−7084.
(38) Zhenyu, S.; Zhanqiang, L.; Hao, S.; Xianzhi, Z. Prediction of contact angle for hydrophobic surface fabricated with micro-machining based on minimum Gibbs free energy. *Appl. Surf. Sci.* **2016**, *364*, 597−603.
(39) Rabuni, M. F. The contrastive study of chemical treatment on the properties of hydrophobic PVDF membrane. *J. Appl. Sci. Process Eng.* **2015**, *2*, 30.
(40) Rabuni, M. F.; Sulaiman, N. M. N.; Aroua, M. K.; Hashim, N. A. Effects of Alkaline Environments at Mild Conditions on the Stability of PVDF Membrane: An Experimental Study. *Ind. Eng. Chem. Res.* **2013**, *52*, 15874−15882.
(41) Nishi, Y.; Iizuka, S.; Faudree, M. C.; Oyama, R. Electrical Conductivity Enhancement of PTFE (Teflon) Induced by Homogeneous Low Voltage Electron Beam Irradiation (HLEBI). *Mater. Trans.* **2012**, *53*, 940−945.
(42) Naughton, M. S.; Brushett, F. R.; Kenis, P. J. A. Carbonate resilience of flowing electrolyte-based alkaline fuel cells. *J. Power Sources* **2011**, *196*, 1762−1768.
(43) Kiaei, Z.; Haghtalab, A. Experimental study of using Ca-DTPMP nanoparticles in inhibition of CaCO3 scaling in a bulk water process. *Desalination* **2014**, *338*, 84−92.
(44) Matty, J. M.; Tomson, M. B. Effect of multiple precipitation inhibitors on calcium carbonate nucleation. *Appl. Geochem.* **1988**, *3*, 549−556.
(45) Zang, L.; Liu, C.-Y.; Ren, X.-M. Adsorption of carbonate and bicarbonate on colloidal silver particles and accompanying optical effects. *J. Photochem. Photobiol., A* **1993**, *74*, 267−271.
(46) Knudsen, J.; Martin, N. M.; Gränäs, E.; Blomberg, S.; Gustafson, J.; Andersen, J. N.; Lundgren, E.; Klacar, S.; Hellman, A.; Grönbeck, H. Carbonate formation on p(4×4)-O/Ag(111). *Phys. Rev. B* **2011**, *84*, No. 115430.
(47) Beckmann, R.; Dulle, K.-H.; Woltering, P.; Kiefer, R.; Funck, F.; Stolp, W.; Kohnke, H.-J.; Helmke, J. Silver Gas Diffusion Electrode

https://doi.org/10.1021/acsaem.1c00715
ACS Appl. Energy Mater. 2021, 4, 5175−5186

for Use in Air Containing CO_2, and Method for the Production Thereof. US2008/0292944 A1, 2008.
(48) Kordesch, K. V. *Hydrocarbon Fuel Cell Technology*; Academic Press, 1965.
(49) Hou, X.; Deem, P. T.; Choy, K.-L. Hydrophobicity study of polytetrafluoroethylene nanocomposite films. *Thin Solid Films* **2012**, *520*, 4916−4920.
(50) García de Arquer, F. P.; Dinh, C.-T.; Ozden, A.; Wicks, J.; McCallum, C.; Kirmani, A. R.; Nam, D.-H.; Gabardo, C.; Seifitokaldani, A.; Wang, X.; Li, Y. C.; Li, F.; Edwards, J.; Richter, L. J.; Thorpe, S. J.; Sinton, D.; Sargent, E. H. CO_2 electrolysis to multicarbon products at activities greater than 1 A cm^{-2}. *Science* **2020**, *367*, 661.
(51) Deluca, N. W. E.; Yossef, A. Nafion/poly(vinyl alcohol) blends: Effect of composition and annealing temperature on transport properties. *J. Membr. Sci.* **2006**, *282*, 217−224.
(52) Li, J.; Yang, X.; Tang, H.; Pan, M. Durable and high performance Nafion membrane prepared through high-temperature annealing methodology. *J. Membr. Sci.* **2010**, *361*, 38−42.
(53) Jalani, N. H.; Datta, R. The effect of equivalent weight, temperature, cationic forms, sorbates, and nanoinorganic additives on the sorption behavior of Nafion. *J. Membr. Sci.* **2005**, *264*, 167−175.
(54) Schulz, K. G.; Riebesell, U.; Rost, B.; Thoms, S.; Zeebe, R. E. Determination of the rate constants for the carbon dioxide to bicarbonate inter-conversion in pH-buffered seawater systems. *Mar. Chem.* **2006**, *100*, 53−65.
(55) Henckel, D. A.; Counihan, M. J.; Holmes, H. E.; Chen, X.; Nwabara, U. O.; Verma, S.; Rodríguez-López, J.; Kenis, P. J. A.; Gewirth, A. A. Potential Dependence of the Local pH in a CO2 Reduction Electrolyzer. *ACS Catal.* **2021**, *11*, 255−263.
(56) Nwabara, U. O.; de Heer, M. P.; Cofell, E. R.; Verma, S.; Negro, E.; Kenis, P. J. A. Towards accelerated durability testing protocols for CO2 electrolysis. *J. Mater. Chem. A* **2020**, *8*, 22557−22571.
(57) Bhargava, S. S.; Proietto, F.; Azmoodeh, D.; Cofell, E. R.; Henckel, D. A.; Verma, S.; Brooks, C. J.; Gewirth, A. A.; Kenis, P. J. A. System Design Rules for Intensifying the Electrochemical Reduction of CO2 to CO on Ag Nanoparticles. *ChemElectroChem* **2020**, *7*, 2001−2011.
(58) Cofell, E. R.; Nwabara, U. O.; Bhargava, S. S.; Henckel, D. E.; Kenis, P. J. A. Investigation of Electrolyte-Dependent Carbonate Formation on Gas Diffusion Electrodes for CO_2 Electrolysis. *ACS Appl. Mater. Interfaces* **2021**, 15132.
(59) Jhong, H.-R.; Tornow, C. E.; Kim, C.; Verma, S.; Oberst, J. L.; Anderson, P. S.; Gewirth, A. A.; Fujigaya, T.; Nakashima, N.; Kenis, P. J. A. Gold Nanoparticles on Polymer-Wrapped Carbon Nanotubes: An Efficient and Selective Catalyst for the Electroreduction of CO2. *ChemPhysChem* **2017**, *18*, 3274−3279.
(60) Verma, S.; Hamasaki, Y.; Kim, C.; Huang, W. X.; Lu, S.; Jhong, H. R. M.; Gewirth, A. A.; Fujigaya, T.; Nakashima, N.; Kenis, P. J. A. Insights into the Low Overpotential Electroreduction of CO2 to CO on a Supported Gold Catalyst in an Alkaline Flow Electrolyzer. *ACS Energy Lett.* **2018**, *3*, 193−198.

https://doi.org/10.1021/acsaem.1c00715
ACS Appl. Energy Mater. 2021, 4, 5175−5186